Journal of Power Sources 234 (2013) 8–15

Contents lists available at SciVerse ScienceDirect

Journal of Power Sources

journal homepage: www.elsevier.com/locate/jpowsour

Graphene nanosheet supported bifunctional catalyst for high cycle life Li-air batteries

Lixin Wang, Mahbuba Ara, Kapila Wadumesthrige [1], Steven Salley [1], K.Y. Simon Ng*,[1]

Dept. of Chemical Engineering and Material Science, Wayne State University, 5050 Anthony Wayne Drive, Detroit, MI 48202, USA

HIGHLIGHTS

- Use graphene as electrochemically stable and highly conductive support matrix.
- $La_{0.5}Ce_{0.5}Fe_{0.5}Mn_{0.5}O_3$ catalyzes the oxygen reduction and evolution reaction.
- 100 cycles, average capacity of 1200 mAh g^{-1} and efficiency of 70% are achieved.

ARTICLE INFO

Article history:
Received 6 October 2012
Received in revised form
21 December 2012
Accepted 7 January 2013
Available online 30 January 2013

Keywords:
Li-air battery
Perovskite catalyst
Graphene cathode
Cycle life

ABSTRACT

Rechargeable lithium-air batteries offer great promise for transportation and stationary applications due to their high specific energy and energy density. Although their theoretical discharge capacity is extremely high, the practical capacity is much lower and is always cathode limited. A key for rechargeable systems is the development of an air electrode with a bifunctional catalyst on an electrochemically stable carbon matrix. The use of graphene as a catalyst matrix for the air cathode has been studied in this work. A Li-air cell using an air cathode consisting of nano-Pt on graphene nanosheets (GNS) has shown promising performance at 80% energy efficiency with an average capacity of 1200 mAh g^{-1} and more than 20 cycles without significant loss of total energy efficiency. Replacement of Pt with a bifunctional catalyst resulted in more than 100 cycles with an average capacity of 1200 mAh g^{-1} and total energy efficiency of about 70%. Electrochemical impedance spectroscopy data revealed increasing solution and charge transfer resistance during cycling, which hindered the cycle life. The increased solution resistance can be attributed to the evaporation and decomposition of electrolyte especially at high charge voltages. Further investigation on ionic liquid based electrolytes in Li-air systems is being conducted.

1. Introduction

Secondary or rechargeable batteries as energy storage devices garner more attention today than at any time in human history due to the pressure to achieve efficient and economical electrification of vehicles and storage of intermittent wind and solar energy. The specific energy of state-of-the-art rechargeable Li-ion battery packs has reached 100–120 Wh kg^{-1} for automotive propulsion applications, and further engineering optimization using currently available chemistry may yield up to about 50% higher values (~180 Wh kg^{-1}). Unfortunately, this is still insufficient to support the long term goals set by USABC in terms of full range (300 miles) electric vehicles because the required ~75 kWh battery would weigh at least 400 kg and thus compromise the vehicle efficiency. Therefore further advances in specific energy are needed but are limited by low capacities of the lithium intercalation compounds used in the cathodes. One promising approach which could achieve at least 4-fold higher energy efficiency is by replacing the Li intercalation cathode with the catalytically active oxygen electrode, forming the so-called Li-air (oxygen) battery, which has the highest specific energy among all known electrochemical couples [1–9]. When only lithium is considered and oxygen is absorbed from the surrounding air environment, the battery has a specific energy of 11,972 Wh kg^{-1} in non-aqueous electrolyte systems. However, Li-air systems suffer from large discharge overpotential (η_{dis}) and charge overpotential (η_{cha}) due to slow kinetics in the oxygen reduction reaction (ORR) and in the oxygen evolution reaction (OER) [8–13]. This corresponds to low cycle life and low electrical energy efficiency, currently on the order of 60–70%. The detailed mechanisms underlying these high over voltages are currently not fully understood, but can be substantially reduced by incorporating

* Corresponding author. Tel.: +1 313 577 3805.
E-mail address: sng@wayne.edu (K.Y.S. Ng).
[1] Alternative Energy Technology Lab, Wayne State University, USA.

0378-7753/$ – see front matter © 2013 Elsevier B.V. All rights reserved.
http://dx.doi.org/10.1016/j.jpowsour.2013.01.037

appropriate catalysts. At the air-electrode (currently porous carbon cathodes), insoluble Li_2O_2 is thought to be formed via the oxygen reduction reaction (ORR). There is some evidence that, with catalysts present, Li_2O_2 will undergo the oxygen evolution reaction (OER) at sufficiently high applied recharge voltages so that the aprotic configuration could be the basis for an electrically rechargeable Li-air battery. However, the insoluble nature of Li_2O_2 in organic electrolytes, make them more prone to clog the porous structure of the air electrode. Although the theoretical discharge capacity of the Li-O_2 cell is extremely high, the practical capacity is much lower and is always cathode limited.

The first challenge is developing an efficient and low cost bifunctional catalyst which reduces both charge overpotential and discharge overpotential. Several bifunctional catalyst systems have been studied [7,13–16], such as electrolytic MnO_2 [7], α-MnO_2 nanowires, Co_3O_4, Fe_2O_3, and $CoFe_2O_4$. These results have demonstrated initial discharge capacities as high as 3000 mAh g^{-1} but declined rapidly after only a few cycles. A steady discharge potential of 2.6 V vs Li^+/Li was observed for all catalysts, however a charge voltage ranging from 4 to 4.7 V was observed, depending on the type of the catalyst used. Lu et al. demonstrated that bifunctional Pt–Au nanoparticles loaded onto Vulcan carbon were shown to enhance the ORR and OER with round trip efficiency of 77% [16]. Pt–Au/C reported in this work demonstrated a discharge capacity of 1200 mAh g^{-1} at a current density of 100 mA g^{-1} with the lowest charging voltage (3.5 V) and highest round-trip efficiency for Li-air cells. However the cycle life of this system was not well studied. In almost all cases, mesoporous carbon has been used as the support for the metal nanoparticles. Such mesoporous carbon supported electrode catalysts have shown quite moderate performance in Li-air batteries, and several major obstacles arising from the carbonaceous air cathode, such as carbon's oxidation in both charge and discharge processes, remain to be overcome if the cycling efficiency and cycle life of Li-air batteries are to be improved.

The second critical research area is the design of a high surface area and chemically stable support matrix for the bifunctional catalyst, which would prevent oxidation during charging. For the practical application of air cathodes, it is critical to choose a carbon matrix with a microstructure providing large surface area and pore volume to facilitate a Li/O_2 reaction and to hold a maximum amount of discharge products which is proportional to the battery capacity per gram of carbon. Among porous carbon materials, Super P [17], Ketjen Black [18–20] and Vulcan carbon [16] with high surface area and pore volumes have been used successfully to achieve high capacity air cathodes. However, during the charge cycle, oxygen is generated in a highly reactive form, causing highly corrosive conditions to the conductive support materials as well as to the carbonate electrolytes. Particularly, high surface area carbon materials used as a conductive support are severely attacked and oxidized (evolving CO_2) under anodic conditions [21]. This suggests that the electrochemical stability of the air cathode support material is a key challenge in the development of practical Li-air systems. As an alternative to highly porous conventional carbon, the use of single walled carbon nanotubes (SWCNT) as support materials for the air electrode has been reported [22]. Recently graphene nanosheets (GNS) as cathode support material have also been used. Bing Sun et al. demonstrated GNS as a better support with some catalytic properties compared to Vulcan XC-72 carbon [23]. An initial discharge capacity of 2332 mAh g^{-1} with an average charge potential of 3.97 V vs Li^+/Li were observed for the GNS based Li-air system. A limited cycling study of GNS (up to only five cycles) showed better performance than Vulcan XC-72 carbon. Similarly, Yoo and Zhou [24] successfully demonstrated GNS as a metal free catalyst support for Li-air batteries. Under a low current density of 0.5 mA cm^{-2}, this system showed performance comparable to a system with Pt/C up to fifty cycles. A recent paper by Peter G. Bruce et al. demonstrated the use of a nano porous gold cathode instead of a carbon based cathode, together with $LiClO_4$/dimethyl sulfoxide electrolyte in a Li-air cell to achieve 100 cycles with 95% capacity retention [9]. However, despite all these research efforts, there is still no viable low cost Li-air system with acceptable discharge capacity, round trip efficiency, and high cycle life. Therefore, research efforts need to focus on improving the capacity retention during cycling. Given the promising stability and enhanced conductivity observed in graphene, we investigated a new Li-air cathode by incorporating bifunctional catalysts into a graphene matrix. The aims of this work are twofold. Firstly, to demonstrate the use of graphene nanosheets (GNS) as an electrochemically stable, highly conductive support matrix for bifunctional catalyst in Li-air cells; and, secondly, the synthesis of novel, low cost bifunctional catalyst of the pervoskite type with the chemical composition $La_{0.5}Ce_{0.5}Fe_{0.5}Mn_{0.5}O_3$ which catalyzes the ORR and OER reactions in a working Li-air cell.

2. Experiment

2.1. Synthesis of graphene nanosheets and anchoring of nano-Pt onto GNS

The incorporation of nanoparticles of bifunctional catalyst onto GNS was performed by two methods. (1) Direct anchoring of catalyst during the synthesis of graphene from graphene oxide. (2) Use of impregnation, and co-precipitation methods to load catalyst onto as-prepared GNS.

Graphite oxide (GO) was synthesized from flake graphite (Asbury Carbons, 230U Grade, High Carbon Natural Graphite 99+) by a modified Hummers' method originally reported by Kovtyukhova et al. [25], in which pre-oxidation of graphite is followed by oxidation with Hummers' method. The pre-oxidation of the graphite power was carried out with concentrated H_2SO_4 solution in which $K_2S_2O_8$ and P_2O_5 were completely dissolved at 80 °C. The pretreated product was filtered and washed on the filter until the pH of filtrate water became neutral. The shiny, dark-gray, pre-oxidized graphite was dried in air overnight. The final oxidation of pre-oxidized graphite was performed by the reaction of pre-oxidized graphite dispersed in chilled H_2SO_4 with slow addition of $KMnO_4$ at a temperature below 20 °C. The resulting thick, dark green paste was allowed to react at 35 °C for 2 h followed by addition of 1 L of DI water to give a dark brown solution. After additional stirring for 2 h, the dark brownish solution was further diluted with distilled water after which H_2O_2 was added slowly until the color of the mixture turned into brilliant yellow. The mixture was allowed to settle overnight and the supernatant was decanted. The remaining product was washed with 10% HCl solution with stirring and the brownish solution was allowed to settle overnight. The supernatant was decanted and the remaining product was centrifuged and washed with DI water.

Pt nanoparticles on graphene nanosheets were synthesized by the ethylene glycol reduction (EG) method following reference [26]. In a typical synthesis, stoichiometric amounts of metal precursors (H_2PtCl_6 as Pt precursor) dispersed in 40 mL ethylene glycol solution and 160 mg GO dispersed in 40 mL ethylene glycol solution are mixed together in a 125 mL round-bottom flask equipped with a N_2 in/outlet. The resulting suspension is refluxed at 403 K for 3 h. The composite mixture was then sonicated for 2 h and then vacuum-filtered until the surface of the composite appeared dry. Then it is washed copiously with acetone and dried at 333 K in a vacuum oven. Finally, the catalyst-GNS composite was heat treated at 473 K under Ar–H_2 (9:1 v/v) gas atmosphere for 2 h. For comparison,

Ketjen Black-supported Pt was also prepared by wet impregnation method. The nominal Pt content on both the graphene and Ketjen Black was 10 wt% each.

2.2. Synthesis of bifunctional catalyst and anchoring of catalyst onto GNS

Perovskite type catalyst, $La_{0.5}Ce_{0.5}Fe_{0.5}Mn_{0.5}O_3$, was prepared by the co-precipitation method mixing stoichiometric amounts of corresponding nitrate compounds in DI water. The precursors were separately mixed in an aqueous solution, and this mixed metal solution was added drop-wise to a new container with an aqueous solution of ammonia to reach a pH value of about 10. The precipitates were filtered, washed with DI water until no pH change could be detected, dried at 110 °C overnight and then calcined in air at 500 °C for 2 h. Synthesized bifunctional catalyst were loaded onto GNS by physical mixing during the slurry preparation.

2.3. Slurry and air cathode preparation

A slurry was prepared using the procedure described by Beattie et al. [5] by mixing catalyst anchored carbon powders (GNS or KB) with 5% PVDF (average MW 534000 GPC, Sigma–Aldrich)/N-methyl pyrolidone (NMP, 99.5%, Sigma–Aldrich) binder mixture and homogenized with a pestle and mortar. Circular disks (1 cm diameter and 1.6 mm thick) were cut from sheets of nickel foam (Goodfellow Corporation) and submerged in the NMP/PVDF/carbon slurry. The disks were sonicated to improve penetration of the carbon matrix on Ni foam. NMP solvent was removed by vacuum drying the carbon coated Ni foam at 110 °C for 12 h. The PVDF binder amount in the final cathode was 10%.

2.4. Material characterization

Raman spectroscopy (Invia Raman Microscope, Renishaw), BET surface area and pore size distribution analyzer (Micromeritics, Tristar III), and SEM (S-2400, Hitachi) were used to characterize as prepared GNS, catalyst/GNS composite, and catalyst/commercial graphene composite. Catalyst composition and structure were analyzed by SEM-EDX and XRD (SmartLab High-Resolution System, Rigaku Corporation).

2.5. Li-air single cell construction and electrochemical characterization

The cell consisted of lithium metal foil as the anode, a 250 μm thick Celgard fiber separator, and a porous cathode constructed from various combinations of carbon matrices and catalyst. 1 M $LiPF_6$ in 1:1 ethylene carbonate: dimethylcarbonate mixture was used as electrolyte. The cell construction was of a spring loaded Swagelok design with active electrode areas of 1.2 cm^2. The cell was assembled in an argon-filled glove box with <1 ppm O_2 and moisture content.

Electrochemical cycling of the assembled cells was done galvanostatically using a Maccor battery cycler (Maccor, Inc, Model 4200) with a cut-off voltage range of 2.0 V–4.8 V while maintaining a constant current density. Electrochemical tests were performed under controlled atmospheric conditions using dry oxygen. To determine the maximum capacity, the first cell was subjected to ~3–5 discharge/charge cycles at a constant current density of 70 mA g^{-1} cathode material. The second cell was used to evaluate for cycle performance using the same rate up to the 60% depth of discharge (DoD) limit. The irreversible capacity loss, coulombic and voltaic efficiency of the cell were recorded as a function of number of charge discharge cycles. The same cell was subjected to Electrochemical Impedance Spectroscopy (EIS) measurements at the 0.1–10^6 Hz frequency range in order to measure the internal resistance build up during discharge–charge cycles.

3. Results and discussion

3.1. Materials characterization

The morphologies of the as-prepared GNS was observed by SEM (shown in Fig. 1). The as-prepared GNS consists of the characteristic wrinkle-like thin nanosheets. The X-ray diffraction pattern of as-prepared GNS is shown in Fig. 2(a). The as-prepared GNS displays both a broad (002) peak and weak (100) peak, implying the breaking of the interplanar carbon bonds of the pristine graphite and the formation of graphene nanosheets. Fig. 2(b) shows the Raman spectrum of the as-prepared GNS and that of graphite. The characteristic sharp D line of crystalline graphite is clearly visible. Two typical Raman peaks of carbon are observed at 1340 and 1585 cm^{-1}, corresponding the D line and G line, respectively. The D line is stronger than the G line, and the D/G intensity ratio in the spectrum is significantly higher than that of well-crystallized graphite, indicating the decrease of the size of the in-plane sp^2 domains and partially disordered crystal structure of graphene nanosheets [23]. The surface area and microstructure of the carbon sources play an important role in the electrochemical performance of Li-air batteries [14,15]. In order to examine the specific surface area and the pore size distribution of the as-prepared GNS and Ketjan Black carbon, N_2 adsorption–desorption isotherm measurements were carried out using Micromeritics, Tristar III surface area and pore distribution analyzer. In Fig. 3(a-1), the GNS is shown to exhibit a typical IV shape, indicating their mesoporous characteristic. The pore size distribution, obtained from the Barrett–Joyner–Halenda (BJH) method, is shown in Fig. 3(a-2). The plot shows that the dominant peaks are in the mesoporous range with a peak around 6 nm. The surface area estimated from the Brunauer–Emmett–Teller (BET) method is 380 $m^2\ g^{-1}$ and the pore volume is 5.49 $cm^3\ g^{-1}$. The nitrogen adsorption/desorption isotherm of Ketjen Black carbon is shown in Fig. 3(b-1). The pore size distribution of Ketjen Black carbon exhibits a mesoporous structure with broad pore size distribution. The surface area estimated from the BET method is 1557.5 $m^2\ g^{-1}$ and the pore volume is 10.5 $cm^3\ g^{-1}$. The discharge capacity of lithium-air batteries is related to the available pore volume of the air electrode [8]. The air electrode can accommodate more discharge products, the discharge time can be longer and the discharge capacity can be higher

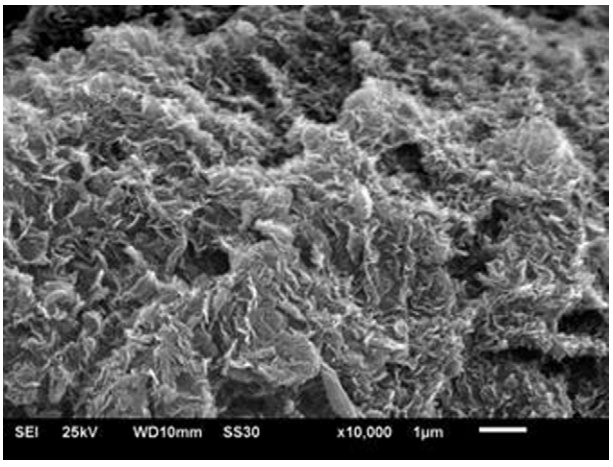

Fig. 1. SEM image of GNS.

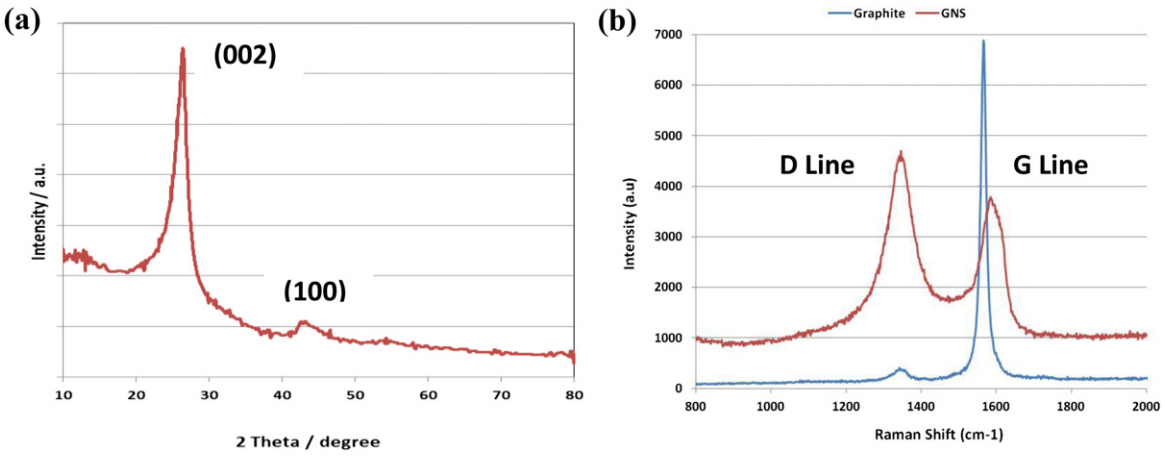

Fig. 2. XRD pattern (a) and Raman spectrum (b) of graphene nanosheets (GNS). For comparison Raman intensity of graphite also included in (b).

if the available pore volume is larger. However, the pore volume and surface area of Pt-GNS was less than the GNS itself and depends on the temperature used to dry the Pt-GNS composite.

3.2. Electrochemical characterization

The electrocatalytic activity of GNS and KB for ORR and OER without added catalysts was examined in Li–O_2 cells and compared with those with added Pt catalysts. The cell configuration was Swagelok type with a carbon coated, 1.6 mm thick and 1 cm diameter Ni foam. The carbon loading on Ni foam was kept constant of at 7 ± 1 mg since the capacity initially increased with the increased carbon loading up to about 12 mg and then decreased drastically with increased carbon loading. The loading of catalyst on carbon was 10%. The discharge/charge cycle (first cycle) of Li-O_2 cells constructed using graphene and KB are shown in Fig. 4. A discharge capacity of 2400 mAh g^{-1} with a nominal discharge voltage of 2.68 V was observed for KB (Fig. 4(a)), while for graphene a discharge capacity of 2000 mAh g^{-1} at a stable nominal discharge voltage of 2.80 V was observed at a constant

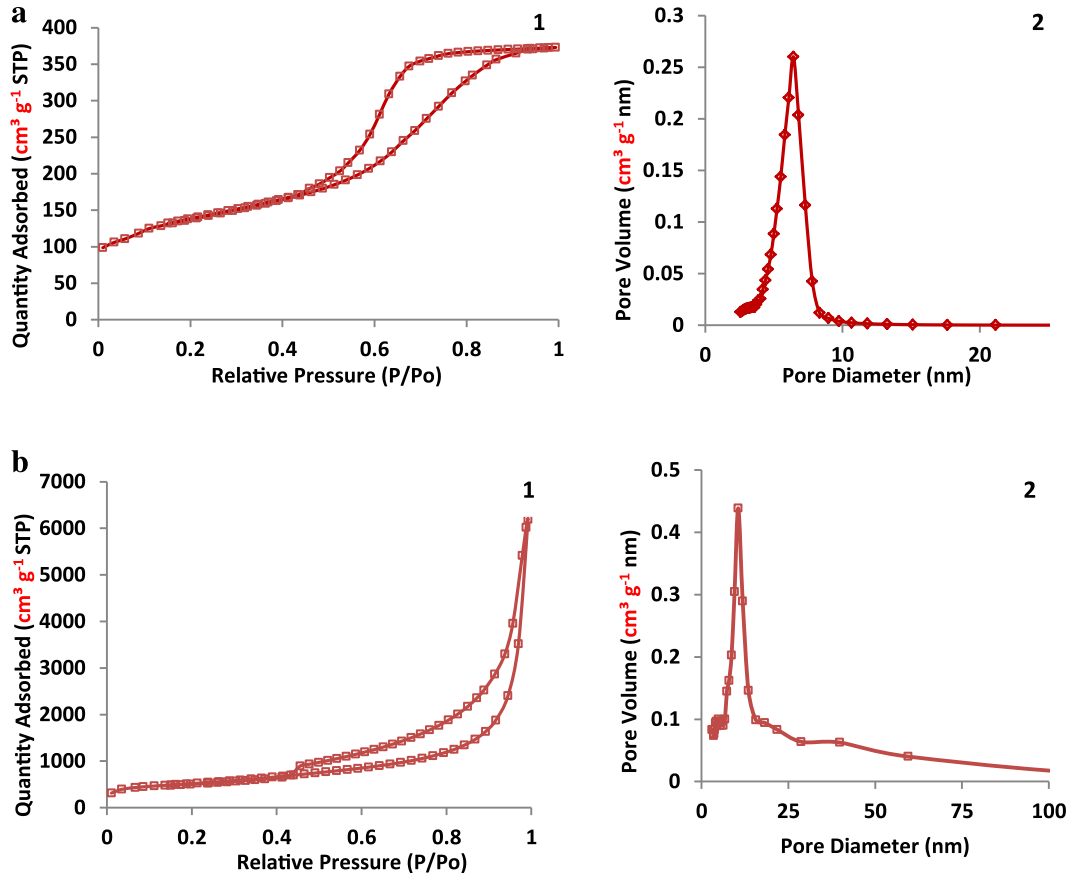

Fig. 3. Nitrogen adsorption–desorption isotherm and pore size distribution curve of GNS (a) and KB (b).

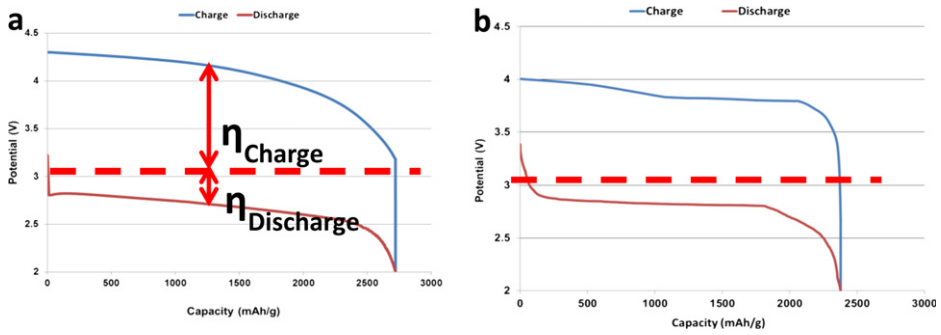

Fig. 4. Discharge and charge curves of graphene (a) and KB (b) based Li-air single cell.

current of 50 mA g^{-1} (Fig. 4(b)). This discharge capacity value reported for KB is comparable to the values reported using porous carbons [17–19]. The lower discharge capacity of GNS compared to KB can be attributed to the lower surface area of synthesized GNS. However, the average charging voltage plateau obtained for GNS (3.90 V) is lower than the value obtained for KB (4.30 V) and values reported using porous carbon without any added catalysts [17,19–22]. The nominal charge and discharge voltages reported here are the average values within the plateau discharge or charge curves (about 95% capacity) and the selected areas are same for all samples. The voltaic efficiency (discharge voltage/charge voltage) for graphene and KB systems are 72% and 63% respectively. Based on the fact that a nearly identical discharge voltage of 2.60 V_{Li} was observed regardless of the type of carbon and for dissimilar catalysts such as Pt and oxides of Fe, Co, Ni, Cu and Mn, Lu et al. [15] concluded that ORR kinetics in Li-air systems is not a catalytically sensitive reaction, or that the ORR kinetics is dominated by the high catalytic activity of different carbon materials. However, we have observed a higher discharge voltage of 2.85 V_{Li} when GNS was used as carbon matrix. This could be due to the higher electrical conductivity of GNS compared to KB containing cells. Similar results were reported by Sun et al. [23] and Yoo and Zhou [24]. The average charge voltage obtained for KB presented in Fig. 4(a) is 4.30 V, which is comparable with the values reported by others. Normally, the charging activity (OER or decomposition of Li_2O_2) of carbon is poor, with an average voltage plateau of 4.70 V_{Li}. The use of catalyzed high surface area carbon can reduced the activation overpotential associated with OER. Average charge voltages of 4.20 V_{Li} on MnO_2/C and 4.00 V_{Li} on gamma MnO_2, alpha MnO_2 nanowires have been observed for catalytic systems. The charge curve of the graphene based cell presented here shows (Fig. 4(b)) a charge voltage even less than 4.00 V_{Li} during the beginning and increased to 4.00 V_{Li} during the latter part of the charge cycle. These observations clearly indicate that GNS catalyzes the OER in Li-air systems. Thus, GNS appears to be a chemically stable, high surface area support material for air cathodes with increased η_{dis}.

The cycling behavior of GNS and KB based cells without added catalysts are shown in Fig. 5. Note that the current density used here was 100 mA g^{-1} and the discharge cycles were terminated when the DoD was 60%. The first cycle discharge capacities at this high discharge rate were 1800 mA g^{-1}, and 1400 mA g^{-1} for KB and GNS respectively. The discharge capacity dropped to 1200 mA g^{-1} within five cycles (14% decreases), while the KB based cell showed a more dramatic capacity drop of 44% after five cycles. The voltaic efficiencies, also presented in Fig. 5, dropped moderately (from 72% to 60%) with the GNS based cell and drastically (from 63% to 30%) with the porous carbon base cell. Although the GNS based lithium air cells showed promising properties over conventional porous carbon based air cathodes, the voltaic efficiencies presented here are still not sufficient for practical applications. Therefore, we have further investigated the incorporation of bifunctional catalysts into GNS and the performance of an air cathode made out of these systems.

Lu et al. [15] showed that bifunctional Au–Pt nano catalysts can greatly influence the discharge and charge voltages of Li-air batteries, where Au is the most active ORR and Pt is the most active for OER. Since the major problems of low cycle life and low voltaic efficiency is due to the slow kinetics of OER, nano scale Pt was impregnated/incorporated into GNS to understand the feasibility of using GNS as a support (host) matrix for bifunctional catalysts. The *in-situ* incorporation of nano scale Pt islands on to GNS was performed by simultaneous reduction of graphene oxide wet impregnated with hexachlorplatinic acid using 5% hydrogen in argon at 450 °C. The SEM image of the Pt-GNS composite with EDX spectrum is shown in Fig. 6(a) and the XRD peaks are shown in Fig. 6(b). The presence of Pt in GNS is characterized by the extra peaks in XRD spectrum. The peaks at $2\theta = 40, 46.2, 68^{\circ}$, and can be assigned to the (111), (200), and (220) crystalline planes of Pt, respectively, which indicates that the Pt nanoparticles are composed of pure crystalline Pt. As evidenced by these data, Pt is attached to GNS.

A Li-air cell made using these cathode materials showed higher electrical efficiency and high cycle life. The discharge capacities and total energy efficiency (voltaic × coulombic) for the Li-air cell consisting of graphene, porous carbon and Pt/graphene cathode are shown in Fig. 7, where graphene demonstrates higher efficiency than conventional porous carbon. With the incorporation of Pt onto

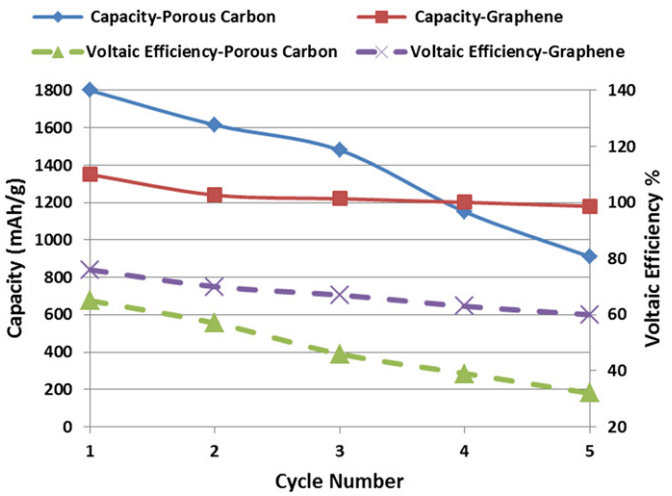

Fig. 5. Comparison of discharge capacity and voltaic efficiency of graphene based and KB based Li-air cells.

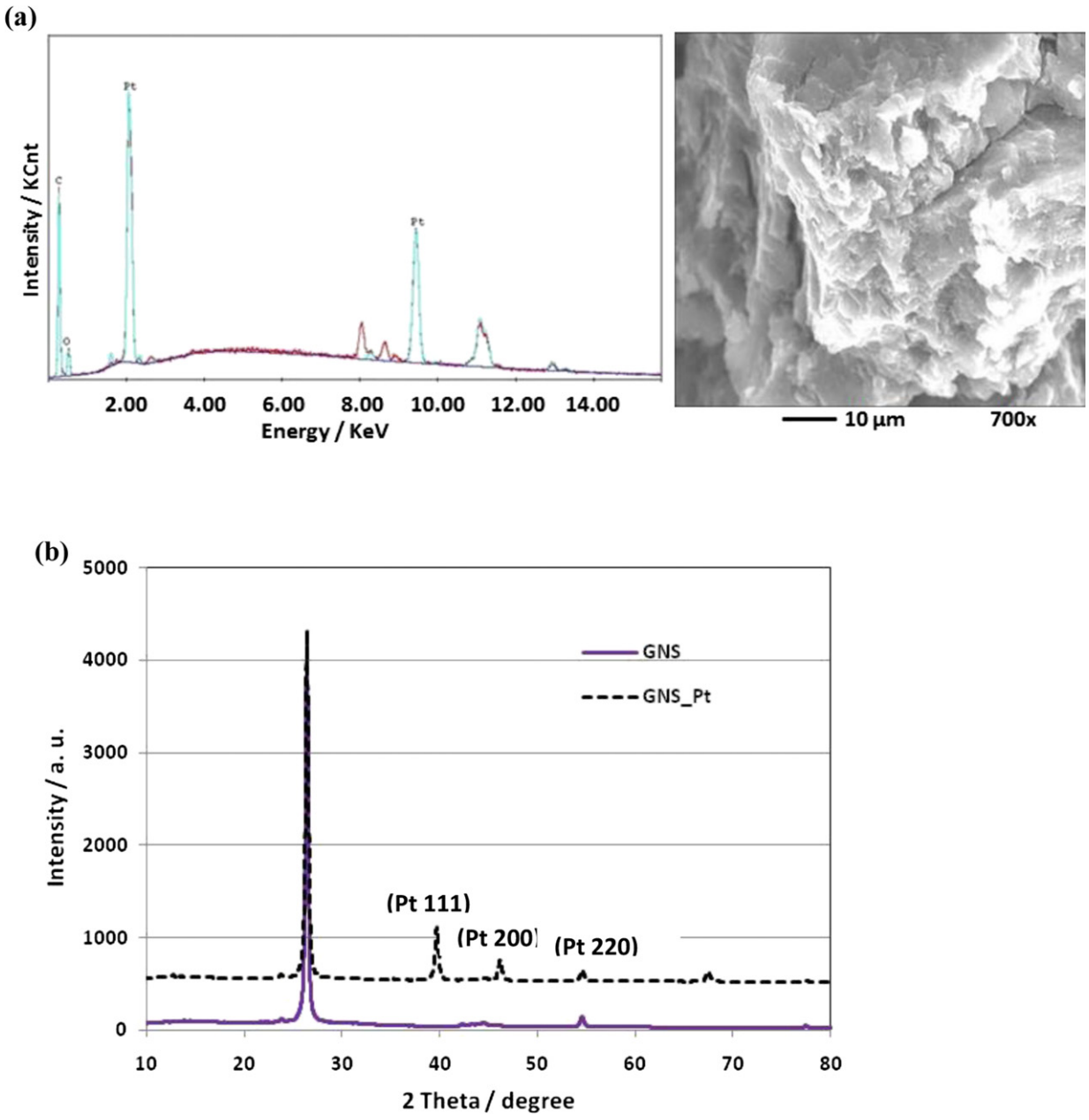

Fig. 6. SEM image with EDX spectrum of Pt anchored on GNS (a) and XRD spectrum of Pt-GNS (b).

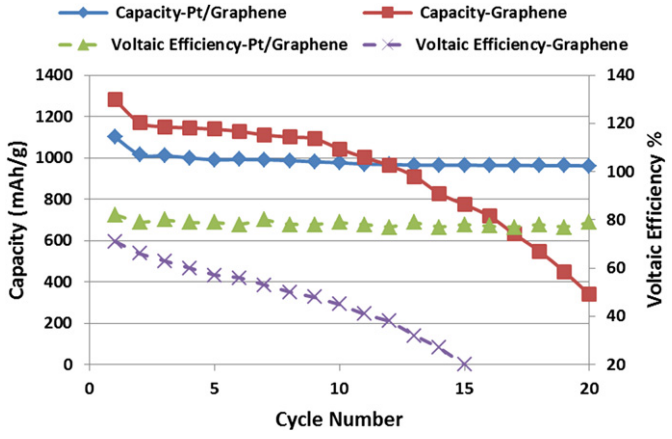

Fig. 7. Comparison of discharge capacity and total energy efficiency of GNS vs Pt/GNS Li-air cells.

GNS the electrical efficiency was about 80%, throughout the number of cycles tested (20 cycles). The nominal discharge and charge voltages for the first cycle for Pt/GNS system were 2.88 V and 3.58 V, respectively. On the other hand, the first cycle nominal discharge and charge voltages for the GNS only system were 2.85 V and 3.92 V, respectively. The voltaic efficiency and discharge capacity for the GNS only system was stable up to about nine cycles, but continuously decreased to 20% and below 400 mAh g^{-1} at the 20th cycle. The discharge voltage dropped slowly during first seven cycles (2.50 V) and then a rapid decrease was observed. However, a continuous increase of charge voltages was observed throughout the cycling. The reasons for the capacity retention till ninth cycle though the voltaic efficiency continued to decrease with cycles is not clear at this point. These data suggested that graphene could be a superior support matrix for bifunctional catalysts for Li-air batteries over conventional carbon.

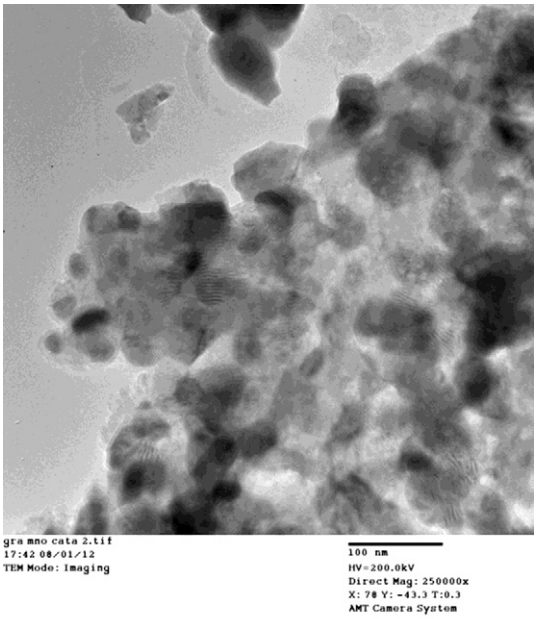

Fig. 8. TEM image of $La_{0.5}Ce_{0.5}Mn_{0.5}Fe_{0.5}$ catalyst on GNS.

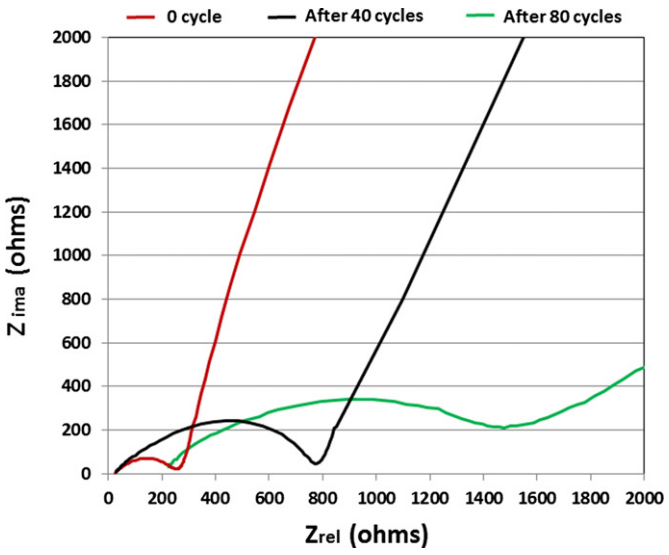

Fig. 10. EIS of $La_{0.5}$ $Ce_{0.5}Fe_{0.5}Mn_{0.5}O_3$/GNS Li-air cells as a function of cycle numbers.

The use of spinel and perovskites mixed metal oxide as bifunctional catalyst for air electrodes for fuel cell applications in aqueous electrolytes has been studied extensively [13]. However, the application of perovskites type bifunctional catalysts in non-aqueous Li-air systems was not studied. Several low cost perovskite type metal oxide catalyst systems have been synthesized and tested in Li-air single cells. The TEM image of $La_{0.5}Ce_{0.5}Fe_{0.5}Mn_{0.5}O_3$ on GNS (Fig. 8) shows that the catalyst particles were well embedded in GNS wrinkles. The size of the irregular shaped catalyst particles ranges from 10 nm to around 50 nm. A cell with the bifunctional catalyst of composition $La_{0.5}Ce_{0.5}Fe_{0.5}Ni_{0.5}O_3$ demonstrated up to 70 cycles without any significant capacity fading. However, the total electrical efficiency was less than 70%. The catalyst with the composition $La_{0.5}Ce_{0.5}Fe_{0.5}Mn_{0.5}O_3$ resulted in an even larger number of cycles with electrical efficiency greater than 75%. The discharge curve for a Li-air cell with this optimized cathode configuration is shown in Fig. 9(a). The cathode material consisted of 10 wt% bifunctional catalyst, 2 wt% binder and the rest GNS. A discharge capacity of 1200 mAh g^{-1} of cathode material at a stable nominal discharge voltage of 2.8 V was observed at a constant current of 50 mA g^{-1}. Several discharge/charge cycles for an identical Li-air cell at a constant current of 100 mA g^{-1} were carried out and the discharge capacity and energy efficiency as a function of cycle numbers are given in Fig. 9(b). A charge voltage of about 3.8 V was observed during the initial cycles; however this charge voltage increased gradually up to a value of 4.20 V at the end of 100 cycles. This gradual increase of charge voltage and gradual decrease of coulombic efficiency resulted in a decrease of electrical efficiency as shown in Fig. 9(b). The cell subjected to discharge/charge at 100 mA g^{-1} after 40th and 100th cycle was further tested for complete discharge/charge at 50 mA g^{-1} and the curves are included in Fig. 9(a). The discharge voltages for these three cycles are almost the same; however the discharge voltage increased with increasing number of cycles. Both discharge and charge curves after cycling exhibited more plateau-like behavior. As expected, the discharge capacity dropped with number of cycles. Further characterization using SEM, EIS, and Raman are underway to understand the failure mechanism which leads to the gradual increase of charge voltage with cycle life.

Electrochemical impedance spectroscopy (EIS) data collected before cycling, after 40 and 80 discharge/charge cycles for the Li-air cell described in Fig. 9(b) are shown in Fig. 10. The increase of ohmic resistance, which includes ionic resistance of electrolyte and electrical resistance from both electrodes (represented by the high frequency intercept of the semi-circle on the real axis) and the

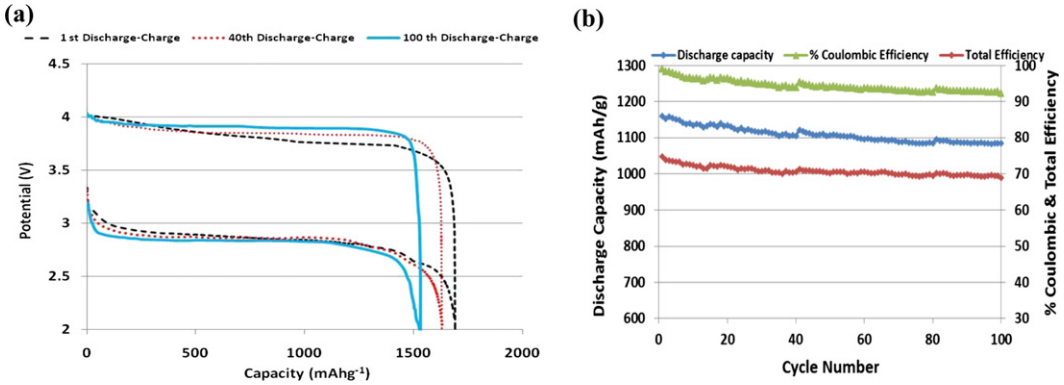

Fig. 9. First discharge and charge curves at 50 mAh g^{-1} until 100% DoD (a); and efficiencies and discharge capacity at 100 mAh g^{-1} with 70–80% DoD (b) of $La_{0.5}$ $Ce_{0.5}Fe_{0.5}Mn_{0.5}O_3$/GNS Li-air cells. Two more discharge and charge curves at 50 mAh g^{-1} after 40th and 100th cycles at 100 mAh g^{-1} also included in (a) for comparison.

increase of the charge transfer resistant (represented by the middle frequency depressed semicircles) as a function of cycle numbers were observed. The reasons for this increasing impedance could be due to the formation of SEI layer or clogging of pores within the carbon matrix which hinder the catalytic activity. Also, it was evident that the drying of electrolyte significantly contributes to the increased ohmic resistance between cycle numbers of 40 and 80. Gao et al. [27] also suggested that the volatilization of organic electrolyte as one of the main factors affecting the discharge capacity when the batteries discharge at low rates (longer times). The use of non-volatile electrolytes such as room temperature ionic liquids may improve the cycle life.

4. Conclusion

The combination of GNS and $La_{0.5}Ce_{0.5}Fe_{0.5}Ni_{0.5}O_3$ bifunctional catalyst as cathode material for air electrode for Li-air system has been demonstrated. This Li-air system exhibited 100 cycles with a charge voltage less than 4 V, with a total efficiency of about 70%. Prevention of decomposition and drying of carbonate based electrolyte may help improve the cyclability.

Acknowledgments

Financial support from the Department of Energy (Grant DE-FG36-05GO85005) for this research is gratefully acknowledged.

References

[1] K.M. Abraham, Z.A. Jiang, J. Electrochem. Soc. 143 (1996) 1–5.
[2] G. Girishkumar, B. McCloskey, A.C. Luntz, S. Swanson, W. Wilcke, J. Phys. Chem. Lett. 14 (2010) 2193–2203.
[3] P.G. Bruce, Solid State Ionics 179 (2008) 752–760.
[4] M. Armand, J.M. Tarascon, Nature 451 (2008) 652–657.
[5] S.D. Beattie, D.M. Manolescu, S.L. Blair, J. Electrochem Soc. 156 (2009) A44–A47.
[6] A.S. Arico, P. Bruce, B. Scrosati, J.M. Tarascon, W.V. Schalkwijk, Nat. Mater. 4 (2005) 366–377.
[7] A. Debart, A.J. Paterson, J. Bao, P.G. Bruce, Angew. Chem. Int. Ed. 47 (2008) 4521–4524.
[8] A. Kraytsberg, Y. Ein-Eli, J. Power Sources 196 (2011) 886–893.
[9] Z. Peng, S.A. Freunberger, Y. Chen, P.G. Bruce, Science 337 (2012) 563–566.
[10] J.S. Hummelshoj, J. Blomqvist, S. Datta, T. Vegge, J. Rossmeisl, K.S. Thygesen, A.C. Luntz, K.W. Jacobsen, J.K. Norskov, J. Chem. Phys. 132 (2010) 071101.
[11] J.P. Zheng, R.Y. Liang, M. Hendrickson, E.J. Plichta, J. Electrochem Soc. 155 (2008) A432–A437.
[12] A. Debart, J. Bao, G. Armstrong, P.G. Bruce, J. Power Sources 174 (2007) 1177–1182.
[13] T. Ogasawara, A. Debart, M. Holzapfel, P. Novak, P.G. Bruce, J. Am. Chem. Soc. 128 (2006) 1390–1393.
[14] Y.C. Lu, H.A. Gasteiger, M.C. Parent, V. Chiloyan, Y. Shao-Horn, Electrochem. Solid State Lett. 13 (2010) A69–A72.
[15] Y.C. Lu, H.A. Gasteiger, E. Crumlin, R. McGuire, Y. Shao-Horn, J. Electrochem. Soc. 157 (2010) A1016–A1025.
[16] Y.C. Lu, Z.C. Xu, H.A. Gasteiger, S. Chen, K. Hamad-Schifferli, Y. Shao-Horn, J. Am. Chem. Soc. 132 (2010) 12170–12171.
[17] H. Cheng, K. Scott, J. Power Sources 195 (2010) 1370–1374.
[18] T. Zhang, N. Imanishi, Y. Shimonishi, A. Hirano, Y. Takeda, O. Yamamoto, N. Sammes, Chem. Commun. 46 (2010) 1661–1663.
[19] J. Xiao, D. Wang, W. Xu, D. Wang, R.E. Williford, J. Elec. Chem. Soc. 157 (2010) A487–A492.
[20] J.G. Zhang, D. Wang, W. Xu, J. Xiao, R.E. Williford, J. Power Sources 195 (2010) 4332–4337.
[21] L. Jorissen, J. Power Sources 155 (2006) 23–32.
[22] G.Q. Zhang, J.P. Zhang, R. Liang, C. Zhang, B. Wang, M. Hendrickson, E.J. Plichta, J. Elec. Chem. Soc. 157 (2010) A953–A956.
[23] B. Sun, B. Wang, D. Su, L. Xiao, H. Ahn, G. Wang, Carbon 50 (2012) 727–733.
[24] E. Yoo, H. Zhou, ACS Nano 5 (2011) 3020–3026.
[25] N.I. Kovtyukhova, P.J. Ollivier, B.R. Martin, T.E. Mallouk, S.A. Chizhik, E.V. Buzaneva, A.D. Gorchinskiy, Chem. Mater. 11 (1999) 771–778.
[26] Z.S. Wu, W. Ren, L. Wen, L. Gao, J. Zhao, Z. Chen, G. Zhou, F. Li, H.M. Cheng, ACS Nano 4 (2010) 3187–3194.
[27] Y. Gao, C. Wang, W. Pu, Z. Liu, C. Deng, P. Zhang, Z. Mao, Int. J. Hydrogen Energy 37 (2012) 12725–12730.